

Unraveling Multimodal Brain Signatures: Deciphering Transdiagnostic Dimensions of Psychopathology in Adolescents

Jing Xia, Nanguang Chen, and Anqi Qiu*

Adolescent psychiatric disorders arise from intricate interactions of clinical histories and disruptions in brain development. While connections between psychopathology and brain functional connectivity are studied, the use of deep learning to elucidate overlapping neural mechanisms through multimodal brain images remains nascent. Utilizing two adolescent datasets—the Philadelphia Neurodevelopmental Cohort (PNC, $n = 1100$) and the Adolescent Brain Cognitive Development (ABCD, $n = 7536$)—this study employs interpretable neural networks and demonstrates that incorporating brain morphology, along with functional and structural networks, augments traditional clinical characteristics (age, gender, race, parental education, medical history, and trauma exposure). Predictive accuracy reaches 0.37–0.464 between real and predicted general psychopathology and four psychopathology dimensions (externalizing, psychosis, anxiety, and fear). The brain morphology and connectivities within the frontoparietal, default mode network, and visual associate networks are recurrent across general psychopathology and four psychopathology dimensions. Unique structural and functional pathways originating from the cerebellum, amygdala, and visual-sensorimotor cortex are linked with these individual dimensions. Consistent findings across both PNC and ABCD affirm the generalizability. The results underscore the potential of diverse sensory inputs in steering executive processes tied to psychopathology dimensions in adolescents, hinting at neural avenues for targeted therapeutic interventions and preventive strategies.


through adolescence.^[1] However, symptoms across psychiatric illnesses appear with high levels of comorbidity,^[2] causing their blurring boundary and making it difficult to diagnose a specific disorder under the current categorical scheme of psychiatric diagnosis.^[3] Such a challenge motivates a shift from a categorical diagnosis to a dimensional view of psychopathology that is characterized by hierarchically ordered and related symptoms, such as externalizing, psychosis, fear, and anxiety, and a general dimension, in a continuous manner.^[4] This dimensional view of psychopathology becomes handy for understanding its risk factors and predictive models in the early onset of psychiatric disorders during adolescence.

Recent studies employed brain images and revealed correlated patterns of psychopathology with brain morphology and structural and functional connectivities.^[5] Increased levels of general psychopathology are associated with less gray matter (GM) in the prefrontal^[6] and temporal cortex^[7] in adolescents and the occipital cortex and cerebellum in adults.^[8] The frontotemporal structural connectivity and crossing fibers in the uncinate fasciculus are associated with general psychopathology in adolescents.^[9] A higher level of general psychopathology maps onto abnormal functional connectivities of the visual associate (VA) cortex with both frontoparietal (FP) and default mode networks (DMNs) in adolescents^[10] and adults.^[5a] These findings suggest that the frontal, visual, and temporal

1. Introduction

Adolescence is a crucial period characterized by brain and psychological development. The incidence of psychiatric illnesses, such as attention deficit hyperactivity disorder (ADHD), anxiety, mood disorders, and psychosis, increases

J. Xia, N. Chen, A. Qiu
 Department of Biomedical Engineering
 National University of Singapore
 Singapore 117583, Singapore
 E-mail: an-qi.qiu@polyu.edu.hk

 The ORCID identification number(s) for the author(s) of this article can be found under <https://doi.org/10.1002/aisy.202300577>.

© 2024 The Authors. Advanced Intelligent Systems published by Wiley-VCH GmbH. This is an open access article under the terms of the Creative Commons Attribution License, which permits use, distribution and reproduction in any medium, provided the original work is properly cited.

DOI: 10.1002/aisy.202300577

N. Chen
 NUS (Suzhou) Research Institute
 National University of Singapore
 Suzhou 215000, China

A. Qiu
 Department of Health Technology and Informatics
 the Hong Kong Polytechnic University
 Hong Kong, Singapore

A. Qiu
 Department of Biomedical Engineering
 the Johns Hopkins University
 Baltimore, MD 21218, USA

regions, supporting executive controls and sensory processing, are engaged in general psychopathology. Whether these structural and functional associations coexist and are *unique* to general psychopathology or *shared across* multiple psychopathological dimensions has not been examined. Existing research is limited to association studies on one brain imaging modality.^[5,10] The putative predictive power of these observed functional and structural associations and clinical characteristics has yet to be well studied in adolescents. Finally, would the pattern of functional and structural associations be replicable across adolescent cohorts?

This study leveraged two large adolescent cohorts, the Philadelphia Neurodevelopmental Cohort (PNC, $n = 1100$) and the Adolescent Brain Cognitive Development (ABCD, $n = 7536$), with comprehensive clinical and brain imaging assessments to address the above questions. We utilized an interpretable neural network framework that examines the predictive power of multimodal brain images (T1-weighted image, resting-state fMRI (rs-fMRI), diffusion-weighted images (DWI)) to general psychopathology and its dimensions in adolescents. It also provides biologically meaningful attention maps explaining correlated patterns of brain imaging signatures (morphology, structural, and functional connectivity) with dimensional psychopathology. Given the strong association between clinical characteristics (such as age, gender, race, parental education, medical history, and trauma exposure) and general psychopathology,^[11] this study expanded upon these traditional clinical features. Using a neural network framework, it assessed the predictive capabilities of brain morphology, along with structural and functional connectivity, either independently or in conjunction with clinical metrics, for general psychopathology. This framework was then applied to transdiagnostic dimensions of psychopathology within the PNC dataset. The validity of identified brain signatures was corroborated by testing their generalizability in another external large dataset (ABCD). The predictive brain signatures allowed us to quantify to extent to which dimensional psychopathology and general psychopathology overlap in the brain. We further evaluated the validity of the brain signature via a meta-analysis of psychiatric disorders using the BrainMap database.

2. Results

2.1. Participants

This study included 1100 youths from the PNC study (Table S1, Supporting Information) and 7536 from the ABCD study (Table S2, Supporting Information). **Table 1** lists the demographic and clinical characteristics, including age, race, gender, parental education, medical history, and trauma exposure. Figure S1, Supporting Information, illustrates their distributions. The PNC study included a wide age range from 8 to 21 years, while the first visit of the ABCD study recruited youths aged from 9 to 11 ($t = 53.2$, $p < 0.001$). There were differences in gender ($\chi^2 = 7.6$, $p = 0.006$), race ($\chi^2 = 71.5$, $p < 0.001$), parental education ($t = -36.3$, $p = 0.001$), medical history ($\chi^2 = 48.7$, $p < 0.001$), and trauma ($\chi^2 = 34.3$, $p < 0.001$) between the two cohorts.

A bifactor model was employed on 117 items of a computerized and structured interview (GOASSESS)^[12] (Table S3, Supporting

Table 1. Demographic and clinical characteristics and psychopathology in the PNC and ABCD cohorts.

Dataset	PNC ($n = 1100$)	ABCD ($n = 7536$)
Age	15.5 \pm 3.4	9.9 \pm 0.6
Gender		
Female	588	3687
Male	512	3849
Race		
European American	47%	56.4%
African American	42.7%	12.2%
Others	10.3%	31.3%
Parental education (years)	14.1 \pm 2.3	16.8 \pm 2.7
Medical history		
No medical problems	26.6%	30.5%
Minor medical problems	51.1%	48.7%
Moderate medical problems	22.3%	19.8%
Trauma	1 \pm 1.22	0.48 \pm 0.92
General psychopathology	11.10 \pm 10.57	3.56 \pm 3.17
Dimensions of psychopathology		
Externalizing	1.27 \pm 1.03	0.31 \pm 0.47
Psychosis	5.39 \pm 6.85	1.41 \pm 1.99
Fear	1.60 \pm 1.46	–
Anxiety	2.41 \pm 2.12	–
Internalizing	–	3.57 \pm 2.84
Suicidality	–	0.12 \pm 0.41
Mania	–	0.69 \pm 1.59

Information) to obtain general psychopathology from p -factor and five psychopathological dimensions, including anxiety, externalizing behavior, fear, psychosis-positive, and psychosis-negative, in the PNC cohort.^[4b] This study created a composite scale of psychosis by combining psychosis-positive and psychosis-negative dimensions comparable with the ABCD measure below. The bifactor model also extracted general psychopathology and five dimensions (i.e., externalizing symptoms, psychosis, internalizing symptoms, suicidality, and mania)^[13] from 84 items of clinical questionnaires and interviews in the ABCD study (Table S4, Supporting Information). Table 1 and Figure S2, Supporting Information, show the descriptive statistics of general psychopathology and dimensional psychopathology in the PNC and ABCD cohorts. The group comparisons on these measures were not conducted as these two cohorts did not use the same tools for assessing child psychopathology.

2.2. The Prediction of General Psychopathology in the PNC and ABCD Cohorts

This study employed neural network approaches on multimodal images to predict general psychopathology in the PNC and ABCD cohorts. **Figure 1A** illustrates the overall framework of multimodal brain image processing and interpretable neural

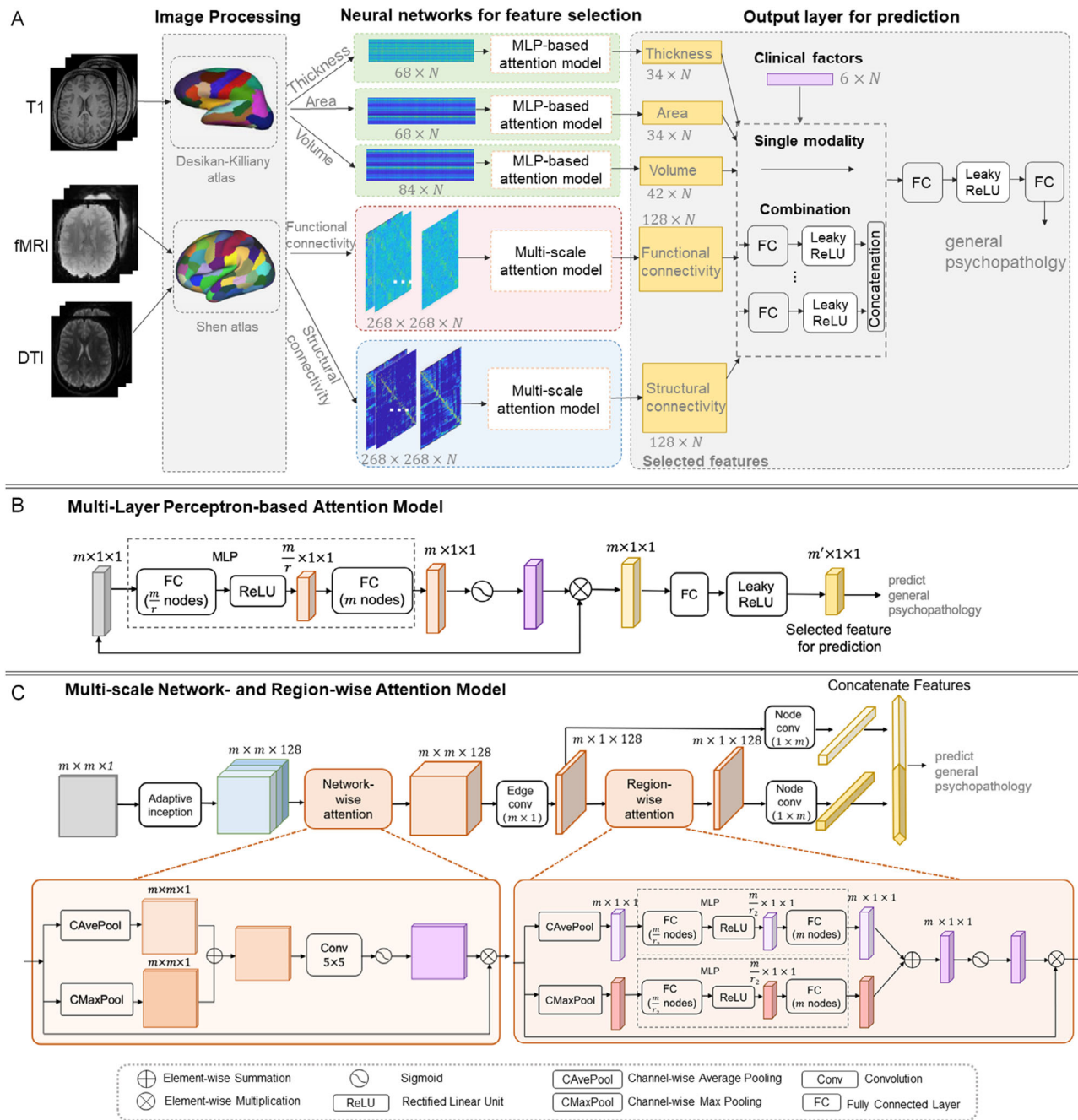


Figure 1. The architectures of neural network methods on multimodal brain images (T1-weighted MRI, rs-fMRI, and diffusion tensor imaging). Panel A) shows the overall framework of the MRI processing, neural networks for feature selection, and the output layer for the prediction of psychopathology. The output layer is designed for predicting general psychopathology in two ways, including using one imaging modality feature and combining multi-modal imaging modality features. Panels B and C) respectively illustrate the architectures of the MLP-based attention model on structural morphology and the multiscale attention model^[19] on structural and functional network data. N is the number of subjects. m is the dimension of input features. Specifically, for cortical thickness, surface area, and volume, m is set as 68, 68, and 84, respectively; for connectome, m is set as 268. r and r_2 are bottleneck ratios in MLP-based attention network and region-wise attention module, and are set as 1.5 and 4, respectively.

networks. This study extracted cortical thickness and surface areas and volumes from T1-weighted images, as well as structural and functional connectivity matrices from DWI and rs-fMRI, respectively. A multilayer perceptron (MLP)-based attention model (Figure 1B) was applied to structural measures

and clinical characteristics, while a multiscale network- and region-attention model (Figure 1C) was employed to structural and functional connectivity for the prediction of psychopathology. **Figure 2** illustrates the prediction accuracy of general psychopathology in terms of Pearson's correlation and

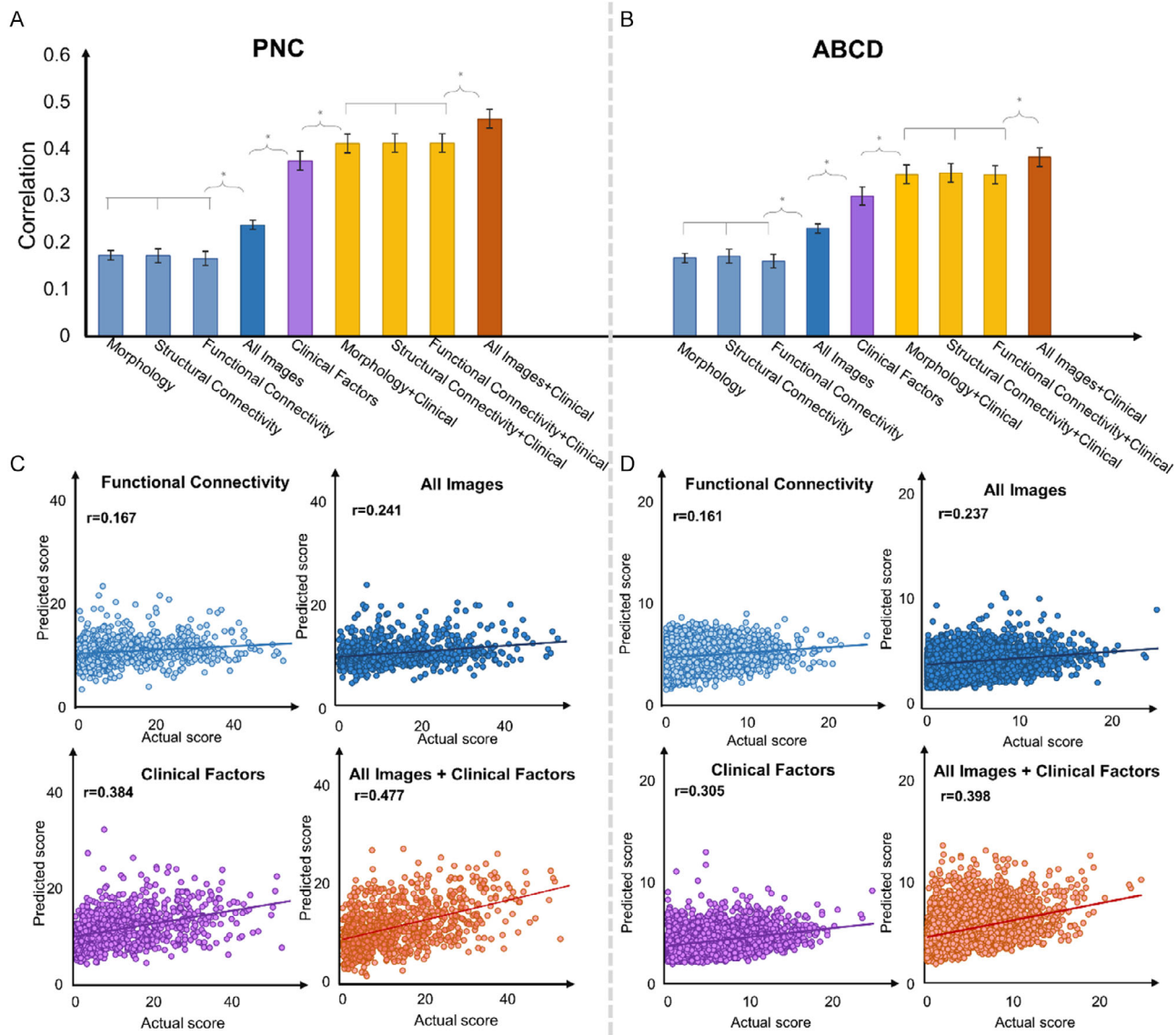


Figure 2. Prediction performance. Panels A,B) show the bar charts of Pearson's correlation coefficients between the actual and predicted general psychopathology over ten runs of fivefold cross-validation on the PNC and ABCD datasets. Panels C,D) illustrate the scatter plots of the actual and predicted general psychopathology scores when using the functional connectivity, three-modal brain images, six clinical factors, and all image features with the six clinical factors on the PNC and ABCD datasets. Blue, dark blue, purple, and red colors represent the performance of the neural networks when using a single image modality, three-modal brain images, six clinical factors, and the combination of the clinical factors with brain images, respectively.

scatter plots between the actual and predicted values of general psychopathology.

For the PNC cohort, single-modal brain images predicted general psychopathology at Pearson's correlation of 0.167–0.172 (blue bars in Figure 2A). There was no significant difference in the prediction power among the three image modalities (Student's *t*-tests: all $p > 0.05$). Our neural network on three imaging modalities predicted general psychopathology at a correlation of 0.237 ± 0.01 (dark blue bar in Figure 2A), significantly improving the prediction power of the single-modal image. In contrast, the prediction model on the six demographic and clinical characteristics (purple bar in Figure 2A) achieved a

correlation of 0.374 ± 0.02 . When the six demographic and clinical characteristics and the image features of functional connectivity, structural connectivity, or morphology were used, the neural network respectively obtained correlations of 0.411 ± 0.02 , 0.412 ± 0.02 , and 0.414 ± 0.02 (yellow bars in Figure 2A). The neural network model with the six demographic and clinical characteristics and the three image modalities achieved the highest correlation of 0.464 ± 0.02 (red bar in Figure 2A) among the above results (blue, purple, and yellow bars in Figure 2A). Figure 2C shows the scatter plots of the actual general psychopathology score and the predicted one from functional connectivity, all three-modal images, demographic and

clinical characteristics, and the combination of the demographic and clinical characteristics as well as all three images. These results indicated that the demographic and clinical characteristics combined with one or multimodal brain images could aid the prediction of general psychopathology.

This study trained the neural networks (Figure 1) based on the PNC cohort and employed transfer learning to evaluate the validity of these neural networks for the ABCD cohort. Since the PNC and ABCD studies did not use the same tools for child psychopathology assessment, transfer learning learned the output layer to calibrate the differences in the psychopathological scales between the two studies. Figure 2B,D show the correlation coefficients and scatter plots between the actual and predicted general psychopathology scores in the ABCD cohort. Single- and three-modal images predicted general psychopathology scores at a correlation of 0.161–0.232, which were comparable with the respective prediction powers on the PNC cohort (all $p > 0.05$) (blue and dark blue bars in Figure 2B). The demographic and clinical characteristics predicted general psychopathology slightly worse in the ABCD cohort ($r = 0.302 \pm 0.02$, purple bar in Figure 2B) than in the PNC cohort ($p < 0.001$). Likewise, the neural networks on the combination of the six clinical characteristics with single- or three-modal images obtained the correlation of 0.349 ± 0.01 , 0.352 ± 0.02 , 0.348 ± 0.02 , and 0.386 ± 0.02 (yellow and red bars in Figure 2B). These findings suggested that the neural networks provided the comparable prediction power of general psychopathology based on brain images but reduced the prediction power of the demographic and clinical characteristics from the PNC to ABCD cohort.

2.3. Attention Maps for the Prediction of General Psychopathology

2.3.1. Clinical Characteristics

This study employed ablation to evaluate the contribution of each clinical characteristic and demonstrated trauma exposure as the most important factor for predicting general psychopathology among the six demographic and clinical characteristics in both the PNC and ABCD cohorts (reduced accuracy by $>25\%$; Figure S3, Supporting Information). Age, gender, and race reduced the prediction accuracy by 1.71%–7.95% (Figure S3, Supporting Information), indicating the variance of general psychopathology partially explained by age, gender, and race. Moreover, dropping the age factor decreased the accuracy of 7.95% in PNC, while 2.06% in ABCD. This difference was caused by the different age ranges of PNC and ABCD, reflecting that age range affects generalizability.

2.3.2. Brain Morphology

Figure 3A and **4A** show the attention maps of the brain morphology and functional and structural connectivity for the PNC and ABCD cohorts, where the attention maps were generated from the neural network shown in Figure 1A. The left panel of Figure 3A illustrates that each morphological measure had its discriminative power in the PNC cohort. The volumes of the left isthmus cingulate cortex, temporal pole, and right banks of the

superior temporal cortex had high attention scores (>0.70). The putamen and amygdala volumes also had high attention scores (>0.76). The thickness of the left fusiform and right precentral gyrus most contributed to the prediction of general psychopathology with attention scores higher than 0.82. Moreover, the area of the left caudal middle frontal, left temporal pole, right supramarginal, and right rostral middle frontal cortex had attention scores greater than 0.73. The left panel in Figure 3B summarizes the frontal, temporal, and cingulate cortex, as well as subcortical regions whose morphology most contributed to the prediction of general psychopathology in the PNC cohort.

The right panels of Figure 3A,B show the attention maps for the ABCD cohort. The overall morphological attention scores of the ABCD cohort highly correlated with those of the PNC cohort ($r = 0.61$, $p < 0.001$; middle panel in Figure 3B), indicating the robust reproducibility of the morphological attention maps across study cohorts.

The average attention scores of the volume, thickness, and area of the highlighted brain regions negatively correlated with general psychopathology (volume: $r = -0.19$, $p < 0.001$; thickness: $r = -0.20$, $p < 0.001$; area: $r = -0.17$, $p < 0.001$) in the PNC study (left panel in Figure 3C). This suggested that reduced brain volumes, surface areas, and cortical thickness predicted a higher general psychopathology score. The same conclusion was seen in the ABCD cohort (the right panel in Figure 3C).

2.3.3. Brain Functional and Structural Networks

For the PNC cohort, the attention maps of the functional and structural networks highlighted the connectivities among the FP, attention (Att), VA, sensorimotor (SM), orbitofrontal (OFC), cerebellar and thalamus-hippocampus (TH) networks that most contributed to the prediction of general psychopathology (purple curves in the left panel of Figure 4A). Beyond the common functional and structural connectivities described above, the functional and structural networks also had specific connections related to general psychopathology (pink and blue curves in the left panel of Figure 4A). The functional connectivities among the DMN, salience (SN) network, and amygdala (Amy) network also exhibited high attention scores. The unique structural connectivities among the cerebellar, TH, and FP networks were highlighted to most predict general psychopathology.

The attention maps of the functional and structural networks in the ABCD cohort were like those in the PNC cohort. They were significantly correlated between the two cohorts (functional connectivity: $r = 0.42$, $p < 0.001$; structural connectivity: $r = 0.38$, $p < 0.001$; the middle column in Figure 4A).

The average attention scores of the highlighted functional connectivity were negatively correlated with general psychopathology in both PNC and ABCD cohorts (PNC: $r = -0.17$, $p < 0.001$; ABCD: $r = -0.16$, $p < 0.001$; Figure 4B). The lower functional connectivity was associated with a greater general psychopathology score. A negative association was also observed in the highlighted structural connectivity and general psychopathology (PNC: $r = -0.16$, $p < 0.001$; ABCD: $r = -0.15$, $p < 0.001$; Figure 4B).

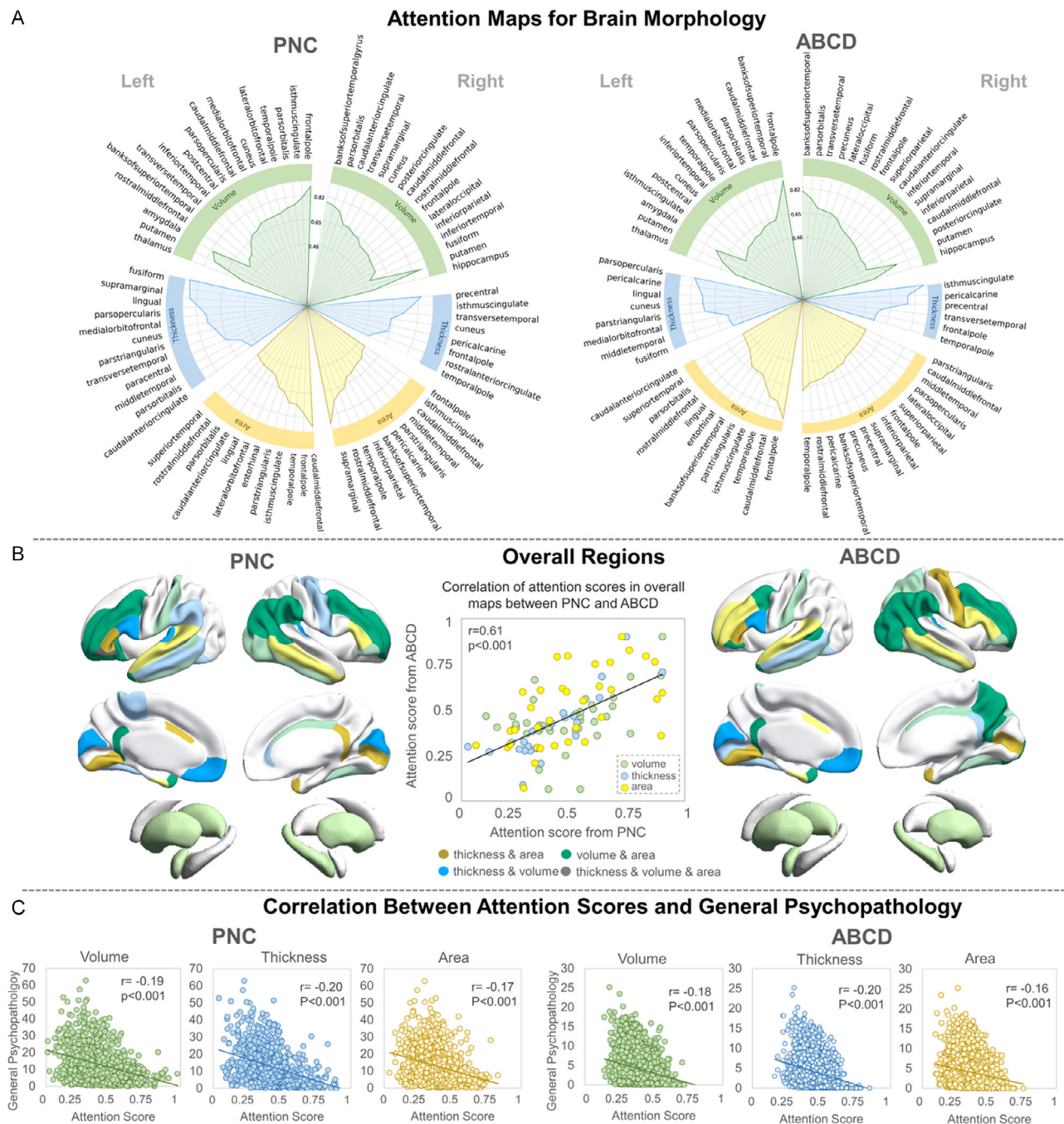


Figure 3. Attention maps of the brain morphology. Panel A) shows the attention maps for the brain volume (green), cortical thickness (blue), and surface area (yellow). In Panel B), the overlap map summarizes the brain regions that were uniquely identified by one morphological measure or shared among all three measures. The left and right panels, respectively, show the overlapping maps for the PNC and ABCD studies. The middle panel shows the correlation of attention scores between the two studies, suggesting the great replicability of the attention maps across cohorts. Panel C) shows the scatter plots of general psychopathology and attention scores for the morphological volume, cortical thickness, and surface area.

2.4. Common and Specific Brain Signatures across Transdiagnostic Dimensions of Psychopathology

The same neural networks on multimodal brain images were applied to the prediction of individual dimensions of psychopathology, including externalizing, psychosis, fear,

and anxiety, in the PNC dataset. The six clinical characteristics predicted them at correlation coefficients of 0.32–0.37 (Figure 5A). When removing trauma from the neural networks, the correlation coefficients were reduced by 41%–49% for the four dimensions of psychopathology (Figure S3, Supporting Information). Age, gender, and race also contributed to their

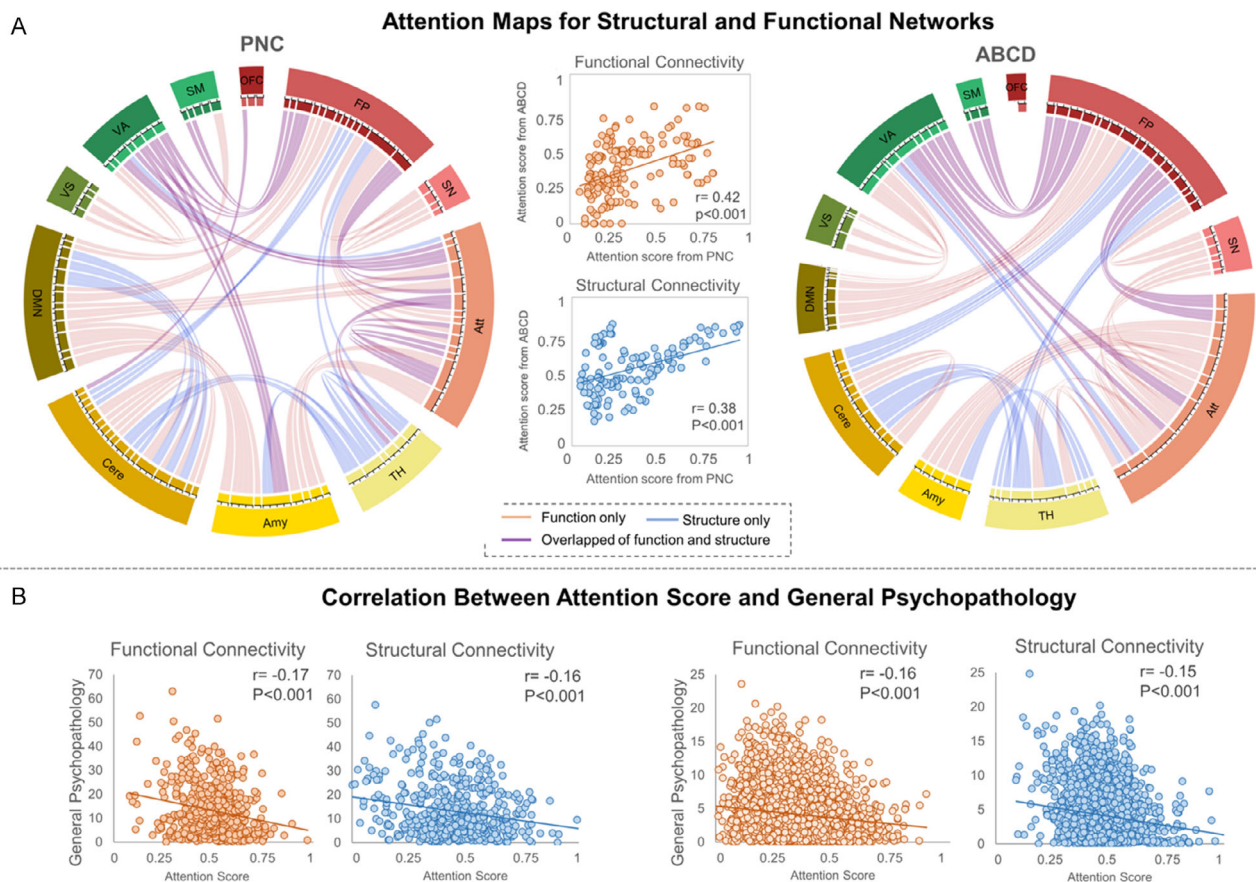


Figure 4. Attention maps of the brain's functional and structural networks. Panel A) shows the attention maps for structural (blue) and functional (red) networks in the PNC and ABCD datasets. The purple lines indicate that both structural and functional connectivities contributed to the prediction of general psychopathology, while orange and light blue lines represent functional and structural connectivities, respectively. Panel B) shows the scatter plots of general psychopathology and the attention scores of functional and structural connectivities.

prediction but with fewer contributions (Figure S4, Supporting Information). These results suggested trauma as the most significant clinical factor contributing to all four psychopathological dimensions. Brain morphology and structural and functional networks predicted externalizing, psychosis, fear, and anxiety at correlations of 0.15–0.2 (Figure 5A). Combining clinical characteristics and three-modal brain images can reasonably predict the four dimensions of psychopathology at correlations of 0.37–0.43 (Figure 5A). These findings suggested that the prediction power of brain images was comparable across the four dimensions of psychopathology. Nevertheless, the attention maps in Figure S5 and S6, Supporting Information, exhibited the common and unique brain regions and networks associated with specific dimensions of psychopathology. The pair-wise correlations among the attention maps of the four psychopathological dimensions ranged from 0.2 to 0.6 on morphology, functional, and structural connectivity (Figure 5B). This implicated that the four dimensions of psychopathology, to a certain extent, shared the common brain morphology, functional and structural networks (gray in Figure 5C), which were highly overlapped with those for general psychopathology (Figure 3B and 4A).

In contrast, the brain images provided specific signatures unique to a particular dimension of psychopathology (Figure 5C). The brain morphology in the right inferior frontal gyrus uniquely contributed to externalizing (orange), in the left posterior-cingulate for psychosis (cyan), in the left amygdala for fear (pink), and in the left precuneus and right superior temporal gyrus for anxiety (brown). Moreover, the functional connectivities between the attention and SM networks and within the visual (VS) network, and structural connectivity between the SN and VA networks uniquely contributed to predicting externalizing. The functional connectivity between the Amy and VA networks, between the cerebellar and FP networks, and the structural connectivity between the SM and SN networks were specific for psychosis. Furthermore, the functional connectivity between the cerebellar and SM networks and the structural connectivity within the Amy network uniquely contributed to fear. Finally, the functional connectivity between the cerebellar and Att networks and between the DMN and Amy networks, and the structural connectivity within the TH network uniquely contributed to anxiety. These results revealed specific structural and functional pathways rooted in the cerebellum, amygdala, visual and SM cortex to individual four psychopathological dimensions.

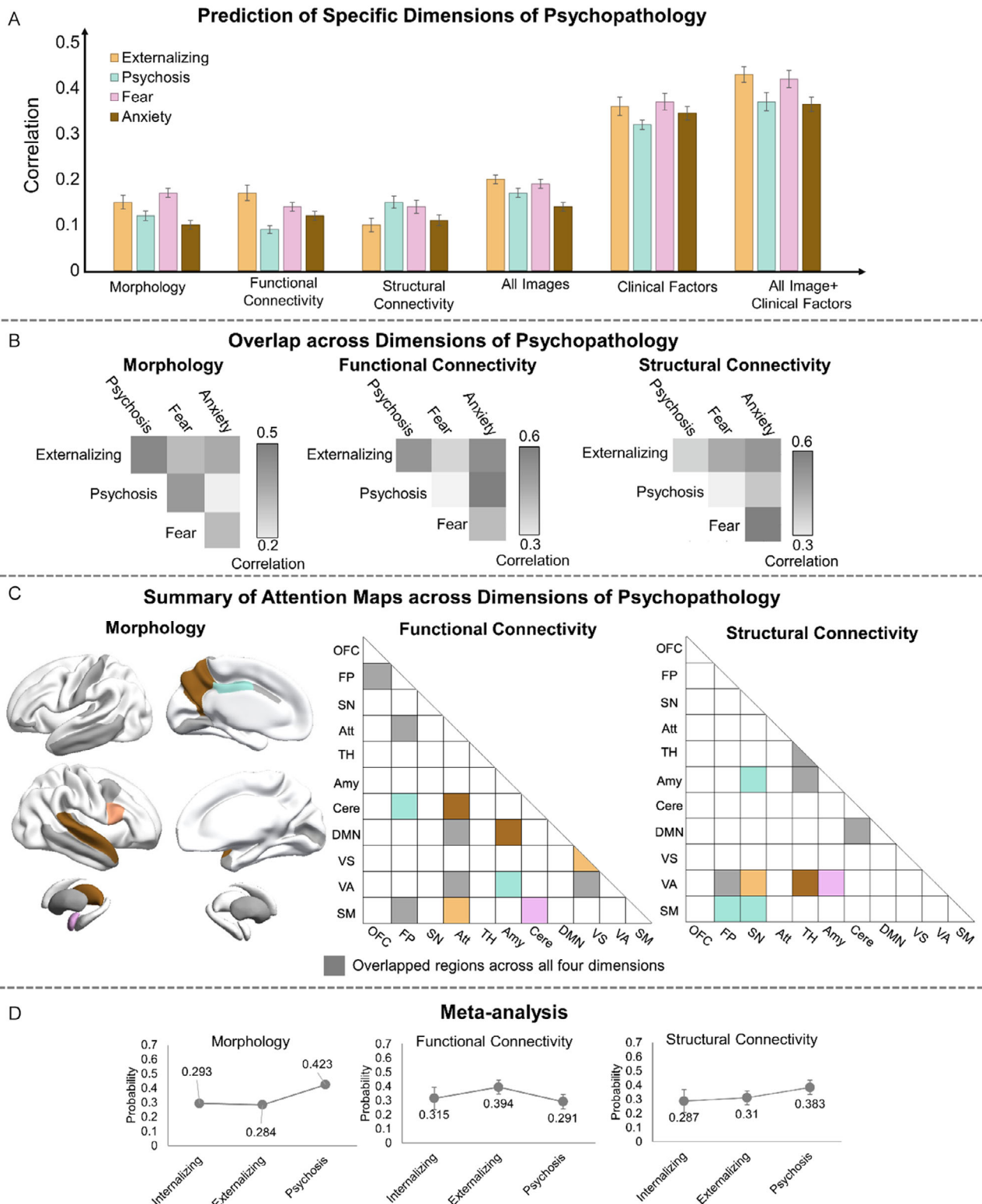


Figure 5. Prediction of dimensions of psychopathology. Panel A) shows the bar charts of Pearson's correlation coefficients between the actual and predicted values of externalizing (orange), psychosis (cyan), fear (pink), and anxiety (brown) based on brain images and six clinical factors for the PNC dataset. Panel B) shows the overlap of image signatures across the four dimensions of psychopathology. The left to right panels, respectively, show the pair-wise correlations of the attention maps of brain morphology, and functional and structural connectivity among the four dimensions of psychopathology. Panel C) summarizes the brain regions and connectivities overlapped across the four dimensions of psychopathology or specific to individual dimensions. Panel D) shows the probability of the morphology, functional connectivity, and structural connectivity that contributed to internalizing, externalizing, and psychosis via meta-analysis on the BrainMap database.

2.5. The Validity of the Attention Maps

The attention maps in Figure 3 and 4 illustrate the validity of the attention maps of general psychopathology identified in both the PNC and ABCD cohorts. Here, we further employed meta-analysis on existing structural and functional MRI studies and examined whether the common brain signatures across the four dimensions of psychopathology equally contribute to these dimensions (see gray in Figure 5C). Due to the lack of existing studies on fear and anxiety in adolescents in the BrainMap database, our meta-analysis combined fear and anxiety as internalizing. Existing studies were extracted from BrainMap based on the keywords in Table S5, Supporting Information, and the age range of 12–25 years. As a result, there were 10 structural and 10 functional studies on internalizing, 24 structural and 47 functional studies on externalizing, and 16 structural and 5 functional studies on psychosis. This study computed the probability of the attention maps in Figure 5C contributed to each transdiagnostic dimension via a Naive Bayes classifier.^[14]

Figure 5D shows that the morphology of the brain regions (gray in the left panel in Figure 5C) contributed to internalizing behavior at a probability of 0.293, externalizing behavior at a probability of 0.284, and psychosis behavior at a probability of 0.423. The regions associated with the shared functional connectivity (gray in the middle panel in Figure 5C) contributed to internalizing behavior at a probability of 0.315, externalizing at a probability of 0.394, and psychosis behavior at a probability of 0.291. The regions associated with the overlapped structural connectivity (gray in the right panel in Figure 5C) contributed to internalizing behavior at a probability of 0.287, externalizing at a probability of 0.310, and psychosis behavior at a probability of 0.383. These results provided additional evidence that the brain features in the attention maps equally contributed to all the dimensions of psychopathology in adolescents, validating the clinical importance of the attention maps.

3. Discussion

This study capitalized on the two large adolescent cohorts and the interpretable neural network framework for predicting adolescent psychopathology. The demographic and clinical characteristics (age, gender, race, parental education, medical history, and trauma exposure) predicted general psychopathology and all four dimensions of psychopathology at a relatively high accuracy. Incorporating brain morphology, along with functional and structural networks, augments traditional clinical characteristics predictive accuracy reaches 0.37–0.464 between real and predicted general psychopathology and four psychopathology dimensions (externalizing, psychosis, anxiety, and fear). Moreover, the morphology, functional and structural networks of FP, DMN, and VA contributed to general psychopathology and shared across the four psychopathological dimensions in adolescents. These findings were replicable in both PNC and ABCD studies and were further validated using meta-analysis on the BrainMap database. Our study provided possible neural mechanisms for effectively leveraging the dimensional view of psychopathology to derive novel targets for clinical intervention and prevention.

This study utilizes a multilevel attention network for connectome features, which are better than other convolution neural network (CNN) based methods and traditional machine learning methods in prediction tasks. CNN-based methods typically treat the connectome as an image and apply convolution operators to it. Kawahara developed BrainNetCNN that introduced edge and node convolution operations according to brain connectivity topology.^[15] BrainNetCNN has demonstrated comparable or superior performance in prediction tasks compared to other CNN-based methods, such as CNN with self-attention.^[16] Connectome predictive modeling^[17] is a machine learning method using linear regression to extract the most relevant features from brain connectivity data for prediction. It can achieve similar results compared with BrainNetCNN.^[18] Building upon the edge and node convolution operators introduced in BrainNetCNN, our framework further utilizes an attention mechanism based on the brain's functional connectivity to identify the most discriminate power features for prediction tasks and to facilitate the enhancement or suppression of functional connectivity's contribution to the prediction. As demonstrated in our previous work,^[19] our framework performed on connectome significantly outperforms BrainNetCNN and other deep learning methods, such as the spatio-temporal graph convolutional network.

Our study identified the FP, DMN, and VA networks whose morphology, structural, and functional connectivities were image signatures for general psychopathology in adolescents. These signatures were also shared across the four psychopathological dimensions, including externalizing, psychosis, fear, and anxiety. Morphologically, the increased levels of general psychopathology were found to be associated with less GM in the prefrontal,^[6,7] temporal,^[7] and cingulate^[8] regions in adolescents. A recent meta-analysis showed a reduced GM volume in the attention and executive control networks shared among schizophrenia, bipolar disorder, depression, addiction, obsessive-compulsive disorder, and anxiety.^[20] Functionally, the functional connectivity of VA with FP and DMN was associated with general psychopathology.^[5] Altered intrinsic functional connectivity of the FP and DMN is linked with a broad category of psychiatric disorders^[21] and general psychopathology.^[10,22] Likewise, a reduced fractional anisotropy (FA) in the cerebello-thalamo-frontal pathway was associated with a higher general psychopathology score,^[23] which was also supported by our findings of the reduced structural connectivity among the FP, subcortical, and cerebellar networks. The FP and DMN networks are linked with executive control, while the VA is involved in cognitive functions related to many forms of psychopathology.^[24] It has been suggested that the VA may play a dominant role in guiding human perception of the external world and constructing internal models necessary for executive controls.^[5] Our findings supported the idea that integrating bottom-up sensory information with executive control processes may be a risk factor for general psychopathology.

From the perspective of brain organization, the FP, DMN, and VA lie in the direction of the functional principal gradient,^[25] suggesting that the brain's principal functional hierarchy is informative to general psychopathology in adolescents.^[21] Moreover, the FP, DMN, and VA also have relatively strong structure–function coupling,^[21,26] supporting their synchronous

alternations in the morphology, structural and functional connectivities predictive of general psychopathology.

The most notable functional-specific connectivity is related to the SN network. The functional connectivity within the SN network is informative to the prediction, explained by a previous study using task-based fMRI,^[27] which indicated that high general psychopathology was associated with reduced activation within the salience network in adolescence. Moreover, we find structural-specific connectivity between the Amy and TH networks contributed to the prediction, which is particularly important in emotional learning^[28] and reported as a common characteristic for several psychiatric disorders, i.e., anxiety^[29] and major depressive disorder^[30] in adolescence.

This study further discovered that specific connections of the cerebellum, VA, SM, and Amy with FP, DMN, and Att are predictive of the psychopathological dimensions. Externalizing was uniquely associated with the connectivity between SM and Att, explained by previous work on reduced local efficiency between attention and motor networks in externalizing behaviors.^[31] Psychosis was associated with the functional connectivity between the amygdala and VA and between the cerebellar and FP networks. The functional connectivity between the amygdala and VA cortex enhances sensitivity and discrimination of perceived stimuli.^[28] The abnormal connectivity between them could reflect processes that result in the misattribution of salience to stimuli in psychosis.^[32] Our findings supported that the alterations of the cerebellar connectivity with the prefrontal cortex were associated with several symptoms of psychosis.^[33] Moreover, fear exhibited the unique contribution of the left amygdala, the functional connectivity between the cerebellum and SM network, and structural connectivity between the VA and Amy networks, confirming the current finding that the cerebellum and amygdala are highly related to fear emotional processing.^[34] For anxiety, the unique contributions of the functional connectivity between the amygdala and DMN further supported the previous hypothesis that amygdala functional organization may be a biomarker of symptoms in generalized anxiety.^[35] Together with the imaging markers related to general psychopathology, our findings may suggest fundamental neural mechanisms for dimensional psychopathology in adolescents. That is, the sensory networks with the FP and DMN could be thought to detect and forward sensory information and generate and update internal models for cognitive tasks. Different psychopathological dimensions may correspond to different sensory information that initializes bottom-up executive processes in adolescents.

To the best of our knowledge, this study developed the attention-based neural network framework to integrate multimodal brain images and automatically detect discriminative brain morphology, and structural and functional connectivities for predicting psychopathology. Our neural network framework achieved a remarkable prediction performance when trained and tested on two large adolescent datasets (PNC and ABCD), highlighting the robustness and reproducibility of our framework. It is also worth noting that our framework can automatically capture important locations of the brain alternations in morphology, structural and functional networks linked with general psychopathology. Such brain locations were also replicable across the PNC and ABCD datasets. The meta-analysis provided

evidence that the brain regions identified by our framework were involved in various forms of mental illness, further highlighting the clinical importance of these imaging signatures.

This study revealed that demographic and clinical characteristics provided the strongest predictions for both general psychopathology and its four dimensions, underscoring the efficacy of current psychopathology assessments. Moreover, this study identified that trauma exposure was the most predictive of general psychopathology and the four psychopathological dimensions among the six demographic and clinical characteristics. It is non-specific to any psychopathological dimensions. This suggested the quick screening of demographic and clinical characteristics, particularly trauma exposure, for identifying risk for general psychopathology in adolescents, followed by obtaining brain images to improve the prediction and identify relevant brain regions for further intervention.

While our results highlighted promising potential applications of our neural network framework for psychopathology prediction in adolescents, our study has several limitations worth considering. First, the age range of the PNC cohort was from 8 to 21 years, while the ABCD cohort was from 9 to 11 years. Second, both PNC and ABCD cohorts used different clinical instruments to assess adolescents' psychopathology. Although this study chose the most matched items across the two datasets, the scales of general psychopathology and its dimensions were different from one cohort to the other. This study employed transfer learning techniques and optimized the output layer to adjust the scale differences across the two cohorts, demonstrating the feasibility of transfer learning to achieve the robust prediction of general psychopathology from one adolescent cohort to the other. However, the performance and robustness of our neural network framework should be further validated on a larger population before any clinical use.

4. Conclusion

In sum, the attention-based neural network framework developed in this study provided a robust and replicable prediction of general psychopathology and its dimensions in adolescents. It could be a potential clinical screening tool for general psychopathology in adolescents. Even speculating, our attention maps highlighted that integrating bottom-up sensory information of the visual cortex with executive control processes may be potential common neural mechanisms across general psychopathology and its dimensions. Nevertheless, different sensory information may initialize executive processes for various dimensions of psychopathology in adolescents. These possible neural mechanisms may effectively leverage the dimensional view of psychopathology to derive novel targets for clinical intervention and prevention.

5. Experimental Section

Participants: PNC: The PNC ($n = 50\,813$) is a large-scale study for understanding interactions among brain development, psychiatric diseases, and genetic factors from preadolescence to early adulthood.^[36] The PNC study was conducted at the Center for Applied Genomics at Children's Hospital of Philadelphia and the University of Pennsylvania's

Brain Behavior Laboratory. Among them, 9498 adolescents aged from 8 to 21 had psychopathology assessments. Only adolescents with minimal health issues and neurological impairments were invited to the neuroimaging investigation following the phenotypic screening. The institutional review boards of the University of Pennsylvania and the Children's Hospital of Philadelphia approved all study procedures.

This study used demographic and clinical characteristics, including gender, race, age, parental education, traumatic events and medical rating, multimodal image data, and psychopathology data from the PNC dataset. This study included participants with no medical condition of the central nervous system and had all three image modalities (i.e., T1, rs-fMRI, and DWI). The rs-fMRI images were selected with mean framewise displacement (FD) within 0.5 mm. As a result, this study included 1100 adolescents (gender: 588 females/512 males; age: 15.5 ± 3.4 years). Table S1, Supporting Information, lists the demographic and clinical characteristics used in this study.

ABCD: The ABCD study is ongoing on adolescents aged 9 to 11 years ($n = 11\,875$; <https://abcdstudy.org/>).^[37] Brain imaging, demographics, environmental factors, and behavioral assessment were assessed at the same visit. Written informed consent was obtained from all parents, and all adolescents provided consent to a research protocol approved by the institutional review board at each data collection site.

This study included adolescents with three image modalities (i.e., T1, rs-fMRI, and DWI) and no central nervous system medical condition (Table S2, Supporting Information). As a result, this study included 7536 participants (3687 females/3849 males).

Child Psychopathology and Its Transdiagnostic Dimensions: For the PNC study, child psychopathology was assessed using a computerized, structured interview (GOASSESS),^[12] adapted from the NIMH Genetic Epidemiology Research Branch Kiddie SADS.^[38] It consists of 117 items regarding anxiety disorders, mood disorders, disruptive behavioral disorders, psychosis symptoms, eating disorders, and substance usage (Table S3, Supporting Information). For participants with less than 30 missing items, R package MICE^[39] was used to impute missing data. This study excluded participants with more than 30 missing items. The bifactor model calculated general psychopathology from the p-factor and five psychopathological dimensions, including anxiety, externalizing behavior, fear, psychosis-positive, and psychosis-negative dimensions.^[4b] This study created a composite scale of psychosis by combining psychosis-positive and psychosis-negative dimensions comparable with the ABCD measure below.

The ABCD study only had 84 items that most matched those used in the PNC study^[40] (Table S4, Supporting Information). The bifactor analysis extracted general psychology via the p-factor and five dimensions (i.e., externalizing symptoms, psychosis, internalizing symptoms, suicidality, and mania).^[13]

MRI Acquisition and Preprocessing: The PNC study collected all MRI scans performed at the Hospital of the University of Pennsylvania by using a single 3T Siemens TIM Trio whole-body scanner. The image acquisition protocol was described in ref. [36]. The brain images of the ABCD study were acquired across 21 sites in the United States with the harmonized imaging protocols for Philips, GE, and Siemens scanners. The details of the image acquisition protocol can be found in ref. [41].

Structural T1-Weighted MRI: The structural image is further processed using FreeSurfer 5.3.0^[42] to segment the brain image into three tissue types, GM, white matter (WM), and cerebrospinal fluid (CSF). Postprocessing quality check is conducted according to the instructions on <https://surfer.nmr.mgh.harvard.edu/fswiki/FsTutorial/TroubleshootingData>. Nonlinear image normalization is achieved by aligning individual T1-weighted MRI images to an atlas space via large deformation diffeomorphic metric mapping (LDDMM).^[43,44] The volume, thickness, and surface area of 68 cortical regions and 16 subcortical volumes are extracted based on the Desikan–Killiany brain registration atlas.^[43]

rs-fMRI: Rs-fMRI was preprocessed with slice timing, zero padding, motion correction, skull stripping, and intensity normalization in FSL.^[46] This study included the scans with mean FD less than 0.5 mm. The whole brain, WM, and CSF signals with six motion parameters were regressed and band-pass filtered (0.01–0.08 Hz). Rs-fMRI was

transformed to its respective T1-weighted image via a boundary-based registration method^[47] and then to the JHU atlas via the transformation obtained from its corresponding T1-weighted image and the atlas image. This study used the brain parcellation with 268 regions of interest (ROIs).^[48] The functional brain network was represented by a functional connectivity matrix of 268×268 , whose element was computed via Pearson's correlation of the time series between two brain regions and Fisher Z-transformation.

DWI: DWIs were first denoised based on principle component analysis (PCA),^[49] and motion-corrupted volumes were visually inspected and removed. Eddy current distortions were corrected with outlier replacement, and intra-volume movement correction was applied.^[50] For each participant, the diffusion tensor model and FA were calculated via dwi2tensor and tensor2metric in the MRtrix3 package. Probabilistic tractography from MRtrix3 package was used to find tracts connecting brain regions. The first diffusion image ($b = 0 \text{ s mm}^{-2}$) was aligned to its corresponding T1-weighted image using rigid-body transformation with 6 degrees of freedom.^[51] DWIs and tracts were brought to the JHU atlas space via LDDMM transformation. The structural connectivity matrix was constructed based on the same 268 brain regions^[48], computed as the number of tracts going through any pairs of brain regions, and normalized by their volumes, resulting in a 268×268 symmetric structural connectivity matrix.

Neural Networks on Clinical Characteristics and Brain Images: This study developed interpretable neural networks on demographic and clinical characteristics and each imaging modality to examine their respective accuracy and robustness in predicting general psychopathology. Figure 1A illustrates the overall framework of image processing and neural network models in this study.

Neural Network for Clinical Characteristics: This study employed six demographic and clinical characteristics, including age, parental education, race, gender, medical history, and trauma exposure. As the dimensionality of the clinical characteristics was low, a simple neural network with two fully connected layers and one leaky rectified linear unit (ReLU) was used to predict general psychopathology. Ablation was used to assess the importance of each clinical characteristic in predicting general psychopathology while removing one factor in the neural network at a time. The percentage of reduction in Pearson's correlation between the actual and predicted values was used as a metric for quantifying the importance of individual demographic and clinical characteristics.

MLP-Based Attention Network for Brain Morphological Measures: This study designed a bottleneck-like MLP attention network on brain morphological measures, such as cortical thickness, surface area, and volume (see Figure 1B). A nonlinear function, ReLU, was included in the bottleneck-like MLP attention network to generate an attention map interpreting brain regions whose morphology contributed most to the prediction of general psychopathology. Specifically, the bottleneck-like MLP incorporates one fully connected layer with a dropout rate of r to reduce the spatial dimension from n nodes to $\frac{n}{r}$ hidden nodes. It then calibrates n nodes from $\frac{n}{r}$ hidden nodes in the second fully connected layer, learning dependencies among all nodes. The region with higher attention weight indicates a larger contribution to the prediction, while a lower value means a lower contribution. Significant morphological regions are enlarged by multiplying the learned attention weights with the input feature, while nonrelated features are compressed.

Multiscale Network- and Region-Attention Models: This study employed a multiscale network- and region-attention network model to learn high-order representations of brain structural and functional networks to predict general psychopathology, as in ref. [19]. As shown in Figure 1C, this deep learning model comprised edge and node convolutional operators, an adaptive inception module, and network-wise and region-wise attention modules. The adaptive inception was designed to learn brain structural/functional networks at multiple spatial scales. The network-wise and region-wise attention modules can learn attention maps from the multiscale structural/functional connectivities at the brain network and regional levels. Specifically, the network-wise attention module performs a convolution operation on the connectivity feature and learns significant subnetworks, while the region-wise attention module utilizes a

bottleneck-like MLP model through a sigmoid function to capture significant regions for prediction. The contribution of related connectome-based markers for prediction is enhanced by using attention modules, while that of nonrelated features is compressed. The selected features were extracted as the input of the output layer described below.

Note that head motion in rs-fMRI was regressed out during the rs-fMRI preprocessing hence was no longer considered in the neural network model.

Output Layer: The output layer was designed in two ways. One was for predicting general psychopathology using one imaging modality or clinical characteristics. The output layer consisted of one fully connected layer with leaky ReLU or without leaky ReLU for predicting psychopathology. The second way was to design the output layer to combine all clinical characteristics and single or multimodal image features. We used one fully connected layer with leaky ReLU for each imaging modality to learn the useful modality-specific features. Subsequently, we concatenated the selected modality-specific features from single or all fully connected layers and the clinical features together into one feature matrix. Following this, another two fully connected layers were employed on the concatenated features for predicting psychopathology (see Figure 1A). Note that, for the combination of all multimodal features, we can repeat the above process without the concatenation of clinical features. The loss function of all the machine learning models was defined as the root mean square error (RMSE) between the actual and predicted values.

Attention Maps: Our neural networks were designed to be interpretable. The MLP-based attention model (Figure 1B) and the multiscale attention model (Figure 1C) were used to compute attention maps for brain morphology and functional and structural connectivity. The greater the value was, the greater the discrimination ability of brain image features was as biomarkers for psychopathology in adolescents.

To evaluate the relationship between the attention module and the general psychopathology scores, regional correlation coefficients between their attention scores and general psychopathology were calculated, as shown in Figure 3C and 4B. Using volume as an example, for each subject j , the attention score A_j of volume is defined as follows

$$A_j = \frac{\sum_{i=1}^K W_{ij} M_{ij}}{\sum_{i=1}^K S_i} \quad (1)$$

here, K is the number of contributed regions (with the highest 50% attention weights) for prediction, and N is the number of subjects. W_{ij} and M_{ij} are the attention weight and volume feature of the i th region of the j th subject, respectively. S_i is the standard deviation of the i th region of N subjects. For each modality, the attention scores of different subjects are normalized to $[0,1]$, by dividing the highest score.

Training and Validation: The PNC was designed as a population-based study, where the distribution of psychopathology was skewed and had a long tail toward its higher score. This study randomly selected 80% of samples from the whole dataset to achieve a relatively uniform distribution of psychopathology. Fivefold cross-validation was employed, where fourfold was used for training (75%) and validation (25%), and onefold was used for testing. The subjects from the same family were assigned to the training, validation, or testing set to avoid data leakage. This process was repeated 10 times. Pearson's correlation between the actual and predicted general psychopathology was used to evaluate the prediction accuracy.

Transfer Learning for Cross-Cohort Validation: This study employed transfer learning from the PNC sample to the ABCD sample in which the prediction model (see Figure 1) was trained using the PNC data. We loaded the neural networks, including the MLP-based attention (Figure 1B) and multiscale network- and region-attention models (Figure 1C) trained on the PNC dataset as pretrained models, and performed them on 60% ABCD data to finetune the parameters and retrain the output layer. The other 20% of the ABCD data was used for validation, while the remaining 20% was reserved for testing.

Transfer learning was necessary in this context because the scale of psychopathology differed between the PNC and ABCD studies due to variations in data acquisition. By employing transfer learning, it became

possible to harmonize the scales of measurements across different cohort datasets. Moreover, the study used the PNC sample to fully train the neural networks because of its large age range, so the trained neural networks were representative of adolescent samples.

Transdiagnostic Dimensions of Psychopathology: We employed the same procedure described above to predict psychopathological dimensions in the PNC study and to examine whether there are unique image signatures related to specific dimensions of psychopathology.

Meta-Analysis on Attention Maps of Psychopathology: We conducted a meta-analysis to evaluate the validity of the attention maps derived from multimodal images via the computation of their contribution to general psychopathology based on the BrainMap database.^[52] The BrainMap database supplies foci Montreal Neurological Institute coordinates for each experiment, which we subsequently mapped into 268 ROIs for function and structure connectivity, along with 68 ROIs for morphology features—all of which were employed in this study. This process achieved several experiments wherein both activated and nonactivated ROIs were identified, thereby signifying their relevance to various dimensions of psychopathology. Here, due to limited studies on general psychopathology, we explored the probability of each attention map contributing to internalizing, externalizing, and psychosis in adolescents.^[14] We extracted existing studies from BrainMap based on the keywords in Table S5, Supporting Information, and the age range of 12–25 years. As a result, we found 10 structural and 10 functional studies on internalizing behavior, 24 structural and 47 functional studies on externalizing behavior, and 16 structural and 5 functional studies on psychosis. Finally, we used the Naive Bayes classifier^[14] to compute the probability of the psychopathology associated with the ROIs generated from the attention modules based on these experiments.

Parameter Setting: MLP-Based Attention Network: The MLP-based attention network employed in this study has a bottleneck ratio (r) of 1.5. The prediction layer for surface area and cortical thickness consists of three fully connected layers with hidden nodes of 68, 34, and 1, respectively. Similarly, the prediction layer for volume includes three fully connected layers with hidden nodes of 84, 42, and 1, respectively. The selected feature was extracted after the first fully connected layer. A dropout layer was incorporated with a dropout rate of 0.2 to enhance regularization. The learning rate was set to 0.01, and the training process spanned 100 epochs.

Multiscale Network- and Region-Attention Models: The adaptive inception module in this study incorporates three types of convolutional filters with kernel sizes of 3×3 , 5×5 , and 7×7 , respectively. These filter kernel sizes were determined empirically through a greedy search among combinations ranging from 2 to 16, such as {2, 4, 8}, {3, 5, 7}, {4, 8, 16}, and so on. Additionally, the number of filters for each filter kernel size was determined via a greedy search from the set {16, 32, 64, 128}. The combination of {32, 32, 32} yielded the best performance for our tasks. As a result, the output of the adaptive inception module has dimensions of $268 \times 268 \times 96$.

The kernel size for the filters in the network-wise attention module is set as 5×5 . Each edge convolutional layer consists of 128 filters, while each node layer also contains 128 filters. In the region-wise attention module, a bottleneck ratio (r) of 4 is employed in the MLP.

The prediction layer consists of three fully connected layers with hidden nodes of 128, 128, and 1, respectively. A dropout layer with a dropout rate of 0.4 is included for regularization. The selected feature is extracted after the first fully connected layer. To handle negative functional connectivity, which is meaningful in this study, Leaky ReLU activation with a leak rate of 0.33 is utilized in all layers. For the training process, the learning rate is set to 0.02, and the network is trained for 30 epochs.

Output Layer: To predict general psychopathology using morphological features and clinical characteristics, the output layer was designed with three fully connected layers. For the selected surface area, cortical thickness, and volume features, the hidden nodes were set as 34, 34, and 42, respectively. Subsequently, two additional fully connected layers were included, with hidden nodes of 64 and 1, to combine the morphological features and clinical characteristics.

In the case of predicting general psychopathology using connectivity features and clinical characteristics, the output layer consisted of a single

fully connected layer with 128 hidden nodes for the selected structural or functional connectivity features. This was followed by two additional fully connected layers with hidden nodes of 64 and 1 to combine the connectivity feature with the clinical characteristics.

For the fusion of all multimodal image features and clinical characteristics, the output layer comprised five fully connected layers. Specifically, the hidden nodes for the selected surface area, cortical thickness, volume, functional connectivity, and structural connectivity features were set as 34, 34, 42, 64, and 64, respectively. To integrate all image features and clinical characteristics for predicting psychopathology, two more fully connected layers were added with hidden nodes of 238 and 1 (refer to Figure 1A). The learning rate was set to 0.01, and the training process spanned 50 epochs.

Implementation: The model is trained using NVIDIA Tesla V100-SXM2 GPU with 32GB RAM and Intel Xeon Gold 5118 CPU with 2.30 GHz and by the stochastic gradient descent algorithm with a mini-batch size of 32. The l_2 -norm regularization rate is set of 1×10^{-3} .

Supporting Information

Supporting Information is available from the Wiley Online Library or from the author.

Acknowledgements

This research/project is supported by STI 2030—Major Projects (no. 2022ZD0209000), the National Research Foundation, Singapore, and the Agency for Science Technology and Research (A*STAR), Singapore, under its Prenatal/Early Childhood Grant (grant no. H22P0M0007). Additional support is provided by the Hong Kong global STEM scholar scheme, and the A*STAR Computational Resource Centre through the use of its high-performance computing facilities. Data used in the preparation of this article were obtained from the Adolescent Brain Cognitive Development (ABCD) study (<https://abcdstudy.org>), held in the NIMH Data Archive (NDA). This is a multisite, longitudinal study designed to recruit more than 10 000 children aged 9–10 and follow them over 10 years into early adulthood. The ABCD study is supported by the National Institutes of Health and additional federal partners under award numbers U01DA041022, U01DA041028, U01DA041048, U01DA041089, U01DA041106, U01DA041117, U01DA041120, U01DA041134, U01DA041148, U01DA041156, U01DA041174, U24DA041123, and U24DA041147. A full list of supporters is available at <https://abcdstudy.org/nih-collaborators>. A listing of participating sites and a complete listing of the study investigators can be found at <https://abcdstudy.org/principal-investigators.html>. ABCD consortium investigators designed and implemented the study and/or provided data but did not necessarily participate in the analysis or writing of this report. This manuscript reflects the views of the authors and may not reflect the opinions or views of the NIH or ABCD consortium investigators.

Conflict of Interest

The authors declare no conflict of interest.

Author Contributions

J.X. and A.Q.: contributed to the study design, data analysis, manuscript writing, and modification. N.C.: contributed to the manuscript writing and revision.

Data Availability Statement

The data that support the findings of this study are openly available in [NIMH] at [<https://doi.org/10.1101/2020.02>], reference number [0].

Keywords

adolescence, neural mechanisms, neural networks, predictive models, psychopathology

Received: September 20, 2023

Revised: March 26, 2024

Published online:

- [1] T. Paus, M. Keshavan, J. N. Giedd, *Nat. Rev. Neurosci.* **2008**, 9, 947.
- [2] a) R. C. Kessler, M. Petukhova, N. A. Sampson, A. M. Zaslavsky, H. U. Wittchen, *Int. J. Methods Psychiatr. Res.* **2012**, 21, 169. b) R. F. Krueger, K. E. Markon, *Annu. Rev. Clin. Psychol.* **2006**, 2, 111.
- [3] F. Edition, *Am. Psychiatr. Assoc.* **2013**, 21, 591.
- [4] a) A. Caspi, R. M. Houts, D. W. Belsky, S. J. Goldman-Mellor, H. Harrington, S. Israel, M. H. Meier, S. Ramrakha, I. Shalev, R. Poulton, *Clin. Psychol. Sci.* **2014**, 2, 119. b) L. Parkes, T. M. Moore, M. E. Calkins, P. A. Cook, M. Cieslak, D. R. Roalf, D. H. Wolf, R. C. Gur, R. E. Gur, T. D. Satterthwaite, *Transl. Psychiatry* **2021**, 11, 232.
- [5] a) M. L. Elliott, A. Romer, A. R. Knodt, A. R. Hariri, *Biol. Psychiatry* **2018**, 84, 452. b) L. Mewton, B. Lees, L. M. Squeglia, M. K. Forbes, M. Sunderland, R. Krueger, F. C. Koch, A. Baillie, T. Slade, N. Hoy, *J. Child Psychol. Psychiatry* **2022**, 63, 734. c) A. L. Romer, M. L. Elliott, A. R. Knodt, M. L. Sison, D. Ireland, R. Houts, S. Ramrakha, R. Poulton, R. Keenan, T. R. Melzer, *Am. J. Psychiatry* **2021**, 178, 174.
- [6] H. R. Snyder, B. L. Hankin, C. A. Sandman, K. Head, E. P. Davis, *Clin. Psychol. Sci.* **2017**, 5, 1001.
- [7] A. N. Kaczkurkin, S. S. Park, A. Sotiras, T. M. Moore, M. E. Calkins, M. Cieslak, A. F. Rosen, R. Ciric, C. H. Xia, Z. Cui, *Am. J. Psychiatry* **2019**, 176, 1000.
- [8] A. L. Romer, A. R. Knodt, R. Houts, B. D. Brigidi, T. E. Moffitt, A. Caspi, A. R. Hariri, *Mol. Psychiatry* **2018**, 23, 1084.
- [9] D. Alnaes, T. Kaufmann, N. T. Doan, A. Córdova-Palomera, Y. Wang, F. Bettella, T. Moberget, O. A. Andreassen, L. T. Westlye, *JAMA Psychiatry* **2018**, 75, 287.
- [10] a) C. H. Xia, Z. Ma, R. Ciric, S. Gu, R. F. Betzel, A. N. Kaczkurkin, M. E. Calkins, P. A. Cook, A. García de la Garza, S. N. Vandekar, *Nat. Commun.* **2018**, 9, 3003. b) Z. Cui, A. R. Pines, B. Larsen, V. J. Sydnor, H. Li, A. Adeimpe, A. F. Alexander-Bloch, D. S. Bassett, M. Bertolero, M. E. Calkins, *Biol. Psychiatry* **2022**, 92, 973. c) N. R. Karcher, G. Michelini, R. Kotov, D. M. Barch, *Biol. Psychiatry Cognit. Neurosci. Neuroimaging* **2021**, 6, 508.
- [11] a) A. Caspi, T. E. Moffitt, *Am. J. Psychiatry* **2018**, 175, 831. b) C. S. Carver, S. L. Johnson, K. R. Timpano, *Clin. Psychol. Sci.* **2017**, 5, 880. c) K. A. McLaughlin, N. L. Colich, A. M. Rodman, D. G. Weissman, *BMC Med.* **2020**, 18, 96.
- [12] M. E. Calkins, K. R. Merikangas, T. M. Moore, M. Burstein, M. A. Behr, T. D. Satterthwaite, K. Ruparel, D. H. Wolf, D. R. Roalf, F. D. Mentch, *J. Child Psychol. Psychiatry* **2015**, 56, 1356.
- [13] L.-K. Pries, T. M. Moore, E. Visoki, I. Sotelo, R. Barzilay, S. Guloksuz, *Biol. Psychiatry Global Open Sci.* **2022**, 2, 283.
- [14] T. Yarkoni, R. A. Poldrack, T. E. Nichols, D. C. Van Essen, T. D. Wager, *Nat. Methods* **2011**, 8, 665.
- [15] J. Kawahara, C. J. Brown, S. P. Miller, B. G. Booth, V. Chau, R. E. Grunau, J. G. Zwicker, G. Hamarneh, *NeuroImage* **2017**, 146, 1038.
- [16] A. Vaswani, N. Shazeer, N. Parmar, J. Uszkoreit, L. Jones, A. N. Gomez, Ł. Kaiser, I. Polosukhin, *Adv. Neural Inf. Process. Syst.* **2017**, 30, 15.

- [17] X. Shen, E. S. Finn, D. Scheinost, M. D. Rosenberg, M. M. Chun, X. Papademetris, R. T. Constable, *Nat. Protoc.* **2017**, 12, 506.
- [18] T. He, R. Kong, A. J. Holmes, M. Nguyen, M. R. Sabuncu, S. B. Eickhoff, D. Bzdok, J. Feng, B. T. Yeo, *NeuroImage* **2020**, 206, 116276.
- [19] J. Xia, N. Chen, A. Qiu, *Med. Image Anal.* **2023**, 90, 102921.
- [20] J. L. R. Andersson, S. N. Sotiropoulos, *NeuroImage* **2016**, 125, 1063.
- [21] a) S. J. Broyd, C. Demanuele, S. Debener, S. K. Helps, C. J. James, E. J. Sonuga-Barke, *Neurosci. Biobehav. Rev.* **2009**, 33, 279.
b) J. W. Buckholz, A. Meyer-Lindenberg, *Neuron* **2012**, 74, 990.
- [22] B. Lees, L. M. Squeglia, L. M. McTeague, M. K. Forbes, R. F. Krueger, M. Sunderland, A. J. Baillie, F. Koch, M. Teesson, L. Mewton, *Biol. Psychiatry* **2021**, 6, 387.
- [23] M. Ito, *Nat. Rev. Neurosci.* **2008**, 9, 304.
- [24] M. P. Austin, P. Mitchell, G. M. Goodwin, *Br. J. Psychiatry* **2001**, 178, 200.
- [25] a) J. Zhu, A. Qiu, *NeuroImage* **2022**, 260, 119482. b) D. S. Margulies, S. S. Ghosh, A. Goulas, M. Falkiewicz, J. M. Huntenburg, G. Langs, G. Bezgin, S. B. Eickhoff, F. X. Castellanos, M. Petrides, E. Jefferies, J. Smallwood, *Proc. Natl. Acad. Sci.* **2016**, 113, 12574.
- [26] a) Z. Gu, K. W. Jamison, M. R. Sabuncu, A. Kucyeski, *Nat. Commun.* **2021**, 12, 4894. b) G. L. Baum, Z. Cui, D. R. Roalf, R. Ciric, R. F. Betzel, B. Larsen, M. Cieslak, P. A. Cook, C. H. Xia, T. M. Moore, *Proc. Natl. Acad. Sci.* **2020**, 117, 771.
- [27] T. D. Shanmugan, D. H. Wolf, M. E. Calkins, T. M. Moore, K. Ruparel, R. D. Hopson, S. N. Vanderkar, D. R. Roalf, M. A. Elliott, C. Jackson, E. D. Gennatas, *Am. J. Psychiatry* **2016**, 173, 517.
- [28] L. Pessoa, R. Adolphs, *Nat. Rev. Neurosci.* **2010**, 11, 773.
- [29] S. Qin, C. B. Young, X. Duan, T. Chen, K. Supekar, V. Menon, *Biol. Psychiatry* **2014**, 75, 892.
- [30] A. Abivardi, D. R. Bach, *Hum. Brain Mapp.* **2017**, 38, 3927.
- [31] G. E. Reimann, A. J. Stier, T. M. Moore, E. L. Durham, H. J. Jeong, C. Cardenas-Iniguez, R. M. Dupont, J. R. Pines, M. G. Berman, B. B. Lahey, *Biol. Psychiatry Global Open Sci.* **2022**, 3, 541.
- [32] M. Jalbrzikowski, V. P. Murty, B. Tervo-Clemmens, W. Foran, B. Luna, *Am. J. Psychiatry* **2019**, 176, 196.
- [33] C. Zhuo, C. Wang, L. Wang, X. Guo, Q. Xu, Y. Liu, J. Zhu, *Brain Imaging Behav.* **2018**, 12, 383.
- [34] T. M. Ernst, A. E. Brol, M. Gratz, C. Ritter, U. Bingel, M. Schlamann, S. Maderwald, H. H. Quick, C. J. Merz, D. Timmann, *Elife* **2019**, 8, e46831.
- [35] E. Makovac, D. R. Watson, F. Meeten, S. N. Garfinkel, M. Cercignani, H. D. Critchley, C. Ottaviani, *Soc. Cognit. Affective Neurosci.* **2016**, 11, 1719.
- [36] T. D. Satterthwaite, J. J. Connolly, K. Ruparel, M. E. Calkins, C. Jackson, M. A. Elliott, D. R. Roalf, R. Hopson, K. Prabhakaran, M. Behr, *NeuroImage* **2016**, 124, 1115.
- [37] D. M. Barch, M. D. Albaugh, S. Avenevoli, L. Chang, D. B. Clark, M. D. Glantz, J. J. Hudziak, T. L. Jernigan, S. F. Tapert, D. Yurgelun-Todd, *Dev. Cognit. Neurosci.* **2018**, 32, 55.
- [38] K. R. Merikangas, S. Avenevoli, E. J. Costello, D. Koretz, R. C. Kessler, *J. Am. Acad. Child Adolesc. Psychiatry* **2009**, 48, 367.
- [39] S. Van Buuren, C. G. Oudshoorn, in *Multivariate Imputation by Chained Equations*, TNO, Leiden **2000**.
- [40] T. M. Moore, E. Visoki, S. T. Argabright, G. E. DiDomenico, I. Sotelo, J. D. Wortzel, A. Naeem, R. C. Gur, R. E. Gur, V. Warrier, *Exposome* **2021**, 2, osac010.
- [41] B. J. Casey, T. Cannonier, M. I. Conley, A. O. Cohen, D. M. Barch, M. M. Heitzeg, M. E. Soules, T. Teslovich, D. V. Dellarco, H. Garavan, *Dev. Cognit. Neurosci.* **2018**, 32, 43.
- [42] B. Fischl, *NeuroImage* **2012**, 62, 774.
- [43] J. Du, L. Younes, A. Qiu, *NeuroImage* **2011**, 56, 162.
- [44] M. Tan, A. Qiu, *IEEE Trans. Image Process.* **2016**, 25, 4061.
- [45] R. S. Desikan, F. Ségonne, B. Fischl, B. T. Quinn, B. C. Dickerson, D. Blacker, R. L. Buckner, A. M. Dale, R. P. Maguire, B. T. Hyman, *NeuroImage* **2006**, 31, 968.
- [46] S. M. Smith, M. Jenkinson, M. W. Woolrich, C. F. Beckmann, T. E. Behrens, H. Johansen-Berg, P. R. Bannister, M. De Luca, I. Drobnjak, D. E. Flitney, *NeuroImage* **2004**, 23, S208.
- [47] D. N. Greve, B. Fischl, *NeuroImage* **2009**, 48, 63.
- [48] a) X. Shen, E. S. Finn, D. Scheinost, M. D. Rosenberg, M. M. Chun, X. Papademetris, R. T. Constable, *Nat. Protoc.* **2017**, 12, 506.
b) E. S. Finn, X. Shen, D. Scheinost, M. D. Rosenberg, J. Huang, M. M. Chun, X. Papademetris, R. T. Constable, *Nat. Neurosci.* **2015**, 18, 1664.
- [49] J. Veraart, D. S. Novikov, D. Christiaens, B. Ades-Aron, J. Sijbers, E. Fieremans, *NeuroImage* **2016**, 142, 394.
- [50] a) J. L. Andersson, M. S. Graham, I. Drobnjak, H. Zhang, N. Filippini, M. Bastiani, *NeuroImage* **2017**, 152, 450. b) J. L. Andersson, S. N. Sotiropoulos, *NeuroImage* **2016**, 125, 1063.
c) J. L. Andersson, M. S. Graham, E. Zsoldos, S. N. Sotiropoulos, *NeuroImage* **2016**, 141, 556.
- [51] a) M. Jenkinson, P. Bannister, M. Brady, S. Smith, *NeuroImage* **2002**, 17, 825. b) M. Jenkinson, S. Smith, *Med. Image Anal.* **2001**, 5, 143.
- [52] A. R. Laird, M. C. Riedel, M. T. Sutherland, S. B. Eickhoff, K. L. Ray, A. M. Uecker, P. M. Fox, J. A. Turner, P. T. Fox, *NeuroImage* **2015**, 119, 70.